

The emergence of the hexagonal lattice in two-dimensional Wigner fragments

Miguel Escobar Azor^{1,2}, Amer Alrakik¹, Louan de Bentzmann¹,
 Xabier Telleria-Allika³, Alfredo Sánchez de Merás⁴,
 Stefano Evangelisti¹, J. Arjan Berger¹

¹Laboratoire de Chimie et Physique Quantiques and European Theoretical Spectroscopy Facility (ETSF), CNRS, Université Toulouse III (UPS), 118 Route de Narbonne, Toulouse, F-31062, France.

²Department of Physics, University of Warwick, Coventry, CV4 7AL, United Kingdom.

³Polimero eta Material Aurreratuak: Fisika, Kimika eta Teknologia saila, Kimika Fakultatea, Euskal Herriko Unibertsitatea, UPV/EHU, and Donostia International Physics Center (DIPC), Donostia, P.K. 1072, 20080, Euskadi, Spain.

⁴Departamento de Química Física, Universitat de València, Dr. Moliner 50, Burjassot, 46100, Spain.

Contributing authors: Miguel.Escobar-Azor@warwick.ac.uk;
amer.alrakik@univ-tlse3.fr; louan.de-bentzmann@univ-tlse3.fr;
xabier.telleria@ehu.eus; Alfredo.Sanchez@uv.es;
stefano.evangelisti@irsamc.ups-tlse.fr; arjan.berger@irsamc.ups-tlse.fr;

Abstract

At very low density, the electrons in a uniform electron gas spontaneously break symmetry and form a crystalline lattice [1]. This type of crystal was first predicted in 1934 by Eugene Wigner and they are thus called Wigner crystals [2]. But which type of crystal will the electrons form? Here we report a numerical study of the density profiles of fragments of Wigner crystals from first principles, i.e., without any empirical data or adjustable parameters. To simulate the Wigner fragments we use Clifford periodic boundary conditions and a renormalized distance in the Coulomb potential [3, 4]. We show that these boundary conditions together with high-spin restricted open-shell Hartree-Fock theory provide a method that can accurately capture the Wigner localisation for systems

with many electrons. We do not make any assumptions about the positions where the electrons will localise. The density profiles we obtain emerge naturally when we minimise the total energy of the system. With our approach we study two-dimensional Wigner fragments with up to 20 electrons. We clearly observe the emergence of the hexagonal crystal structure which has been predicted to be ground-state structure of the two-dimensional Wigner crystal.

In 1934 Eugene Wigner argued that in a uniform gas of electrons the Coulomb repulsion is dominant with respect to the kinetic energy when the average density is sufficiently low [2]. Therefore, he predicted that the system would naturally break its translational invariance with the electrons localizing at fixed positions in space thus forming a crystal. *But which type of crystal would the electrons form?* It was later predicted that in one dimension the electrons would form a linear chain, in two dimensions they would form a hexagonal (or triangular) lattice and in three dimensions a body-centred cubic lattice. All these predictions were based on the comparison of the energies for a few known crystal structures [2, 5–13]. For example, in two dimensions it can be shown that the hexagonal lattice has a lower energy than the square lattice. However, this leaves open the possibility that there might be another, less trivial, lattice structure that has a lower energy than the hexagonal lattice [14]. In this work we make an important step towards the prediction of the lattice structure of Wigner crystals *without* making any assumptions about the lattice structure. We achieve this by spatially confining the electrons at very low (average) density and minimizing the total energy using a variational approach to find the electronic wave function of the ground state. The electronic density corresponding to this wave function then corresponds to the lowest-energy configuration of the electrons. In this work we will study fragments of Wigner crystals in which the translational symmetry of the crystal is retained. We will therefore refer to these systems as Wigner fragments [15]. We will show that, in two dimensions, when increasing the number of electrons, there is a clear emergence of the hexagonal crystal structure in the Wigner fragments.

Recently, a two-dimensional Wigner crystal has been observed experimentally by Smolenski and coworkers [1]. However, they did not determine the lattice structure. Two-dimensional crystal lattices consisting of electrons have also been obtained in other experiments, mainly by using magnetic fields or Moiré superlattices [16–27]. In the literature, these systems are also frequently called Wigner crystals. Closely related to the Wigner fragments studied here, are Wigner molecules, in which the electrons are typically confined by an external potential which breaks the translational invariance of the electron gas [28–37]. Wigner molecules have also been observed experimentally [38–41].

In some recent works, we presented Clifford periodic boundary conditions and a renormalized distance as a simple and efficient approach to describe periodic Coulomb systems [3, 4, 13, 42]. Amongst other applications, we applied our approach to describe the Wigner localisation of two electrons in one, two, and three dimensions using a regular grid of gaussian basis functions in a large supercell that has the topology of a

Clifford torus [4]. In this work we present a general approach that can treat Wigner fragments with, in principle, any number of electrons.

Wigner fragments and the Clifford torus

We consider an electron gas confined to a two-dimensional Clifford torus. To be more precise, we define a rectangular 2-dimensional supercell containing a fragment of an electron gas, and then modify its topology into that of a torus by joining opposite sides of the supercell *without deformation*. This procedure yields a supercell that has the topology of a 2-dimensional Clifford torus, which is a flat, closed 2-dimensional real Euclidean space embedded in a 2-dimensional complex Euclidean space. Therefore, we refer to this supercell as the Clifford supercell. The most important property of the Clifford torus is its flatness, i.e., it has zero gaussian curvature everywhere. As an illustration, we report in Fig. 1 the rectangular representation of a 2-dimensional Clifford torus. More details of our approach based on Clifford periodic boundary conditions can be found in Ref. [4].

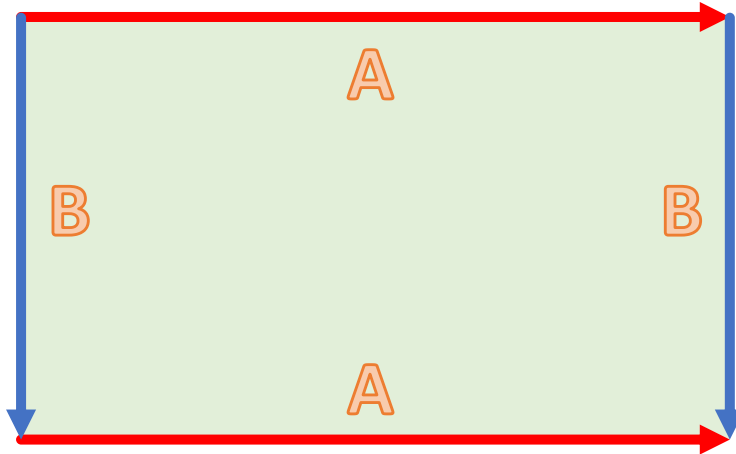


Fig. 1 A representation of a 2-dimensional Clifford torus. Its fundamental polygon is a rectangle. In a Clifford torus opposite sides are joint without deformation.

The Hamiltonian of N electrons confined to the Clifford torus, in Hartree atomic units, is given by

$$\hat{H} = -\frac{1}{2} \sum_{i=1}^N \nabla_i^2 + \frac{1}{2} \sum_{i=1}^N \sum_{\substack{j=1 \\ j \neq i}}^N \frac{1}{r_{ij}}, \quad (1)$$

where the first term on the right-hand side is the kinetic-energy operator of the electrons and the second term is the Coulomb repulsion between the electrons. The Coulomb potential is defined in terms of the Euclidean distance r_{ij} which is the distance between electrons i and j in the embedding space of the Clifford torus. This ensures that all derivatives of the Coulomb potential are continuous everywhere in

the Clifford supercell. We note that this is not the case if r_{ij} would be defined as the distance *on* the Clifford torus [42]. In two dimensions this renormalized distance is defined as

$$r_{ij} = \frac{1}{\pi} \sqrt{L_x^2 \sin^2 \left[\frac{\pi}{L_x} (x_i - x_j) \right] + L_y^2 \sin^2 \left[\frac{\pi}{L_y} (y_i - y_j) \right]}, \quad (2)$$

where L_x and L_y are the lengths of the edges of the Clifford supercell.

High-spin configuration and the Hartree-Fock method

To obtain the lowest-energy configuration of the electrons at low electronic density, one could solve the time-independent Schrödinger equation with the Hamiltonian given in Eq. (1). From the wave function corresponding to the lowest energy eigenvalue, the positions where the electrons localise can be obtained. However, such a calculation is numerically feasible only for very few electrons. Therefore, we have to find a numerically more efficient approach that can capture the electron localisation at low density. We make use of two properties of the uniform electron gas in the low-density limit. In this limit 1) the electrons behave as a single particle, since fixing the position of one electron uniquely determines the positions of all the others [31, 43]; 2) the spin configuration of the wave function becomes irrelevant, i.e., all spin configurations become degenerate. As a consequence, at very low density, we can focus on the high-spin state, which has the maximum value for the spin projection $|S_z|$. The advantage of this spin state is that it can be described with a single Slater determinant by fixing the position of a single electron. A Schrödinger equation for which the solution is a single Slater determinant can be solved with the Hartree-Fock method. More precisely we will use the restricted open-shell Hartree-Fock (ROHF) approach.

In practical calculations we have to project the Hartree-Fock equations onto a basis set. We use a gaussian basis that is distributed regularly in the Clifford supercell to perform our numerical calculations. All gaussians have the same exponent that is adapted to the size of the supercell in such a way to have an overlap between nearest neighbours that is sufficiently large to accurately describe the wave function but not too close to unity, in order to avoid numerical problems due to quasi-linear dependence. We have shown that the overlap between nearest neighbours is proportional to the parameter $\xi = \alpha\delta^2$ in which α is the exponent of the gaussian and δ the nearest neighbour distance between the gaussians [44]. Unless stated otherwise, we used 400 gaussians on a 20×20 grid and $\xi = 0.8$. We have implemented our approach in the DALTON software package [45]. All calculations on two-dimensional (2D) Wigner crystals have been performed at a Wigner-Seitz radius r_s equal to 105. This is well above the theoretically predicted value of $r_s = 31$ for the Fermi liquid to Wigner crystal phase transition in two dimensions [8, 9, 12]. Without loss of generality, we accelerated the convergence of the calculations by adopting the following protocol: 1) we performed a first calculation in which we fix one electron by adding a small positive charge in the origin of the Clifford supercell; 2) we then performed a second

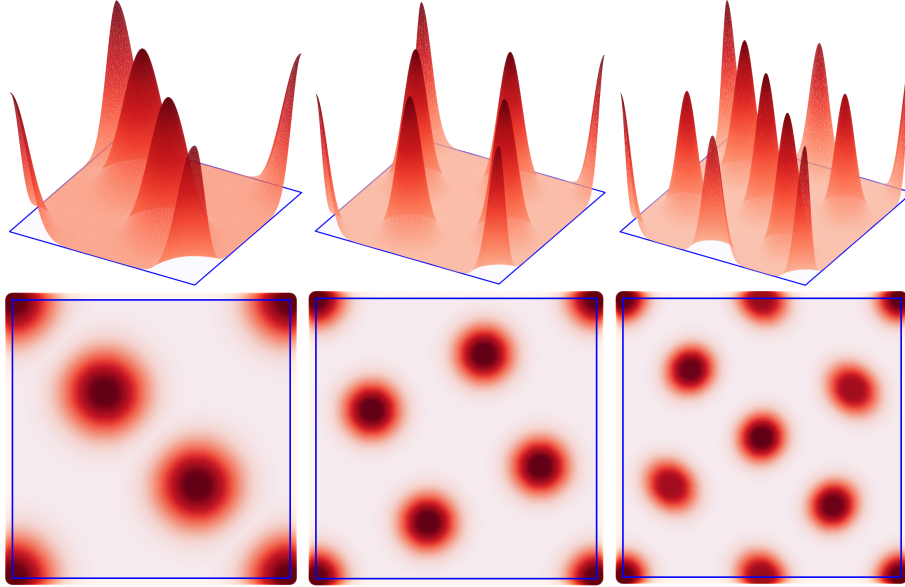


Fig. 2 The density profiles of 3 (left panel), 5 (middle panel) and 7 (right panel) electrons confined to a 2D square Clifford supercell at $r_s = 105$. The profiles on the top show a view from the front while the profiles at the bottom show a view from above.

calculation without the small positive charge using the density of the first calculation as a starting point.

The emergence of the hexagonal lattice

Before reporting the results on 2D Wigner fragments, we note that we have done preliminary work on one-dimensional (1D) Wigner fragments. In particular, we verified numerically that in the low-density limit the wave function indeed becomes mono-determinantal. We achieved this by performing accurate multi-configurational calculations using the complete-active-space self-consistent field (CASSCF) method [46] on 2 electrons confined to a Clifford supercell of length L . We found that at extremely low density ($r_s = 25\,000$) the occupation numbers of the lowest two spin-orbitals are 0.99975 using a CAS(2,4). This confirms that in the low-density limit the ground-state wave function can be described by a single Slater determinant.

In the left panel of Fig. 2 we report the electron density of a Wigner fragment with three electrons confined to a square Clifford torus. We observe that the electrons localise on the diagonal of the Clifford supercell. The three-electron 2D system thus behaves as a 1D system with length $L = \sqrt{L_x^2 + L_y^2}$. We note that the reported solution is degenerate with another solution in which the electrons localise on the other diagonal of the Clifford supercell. In the following, for the sake of simplicity, we will avoid discussing the degenerate solutions we have obtained, since the density profiles of all degenerate solutions are equivalent.

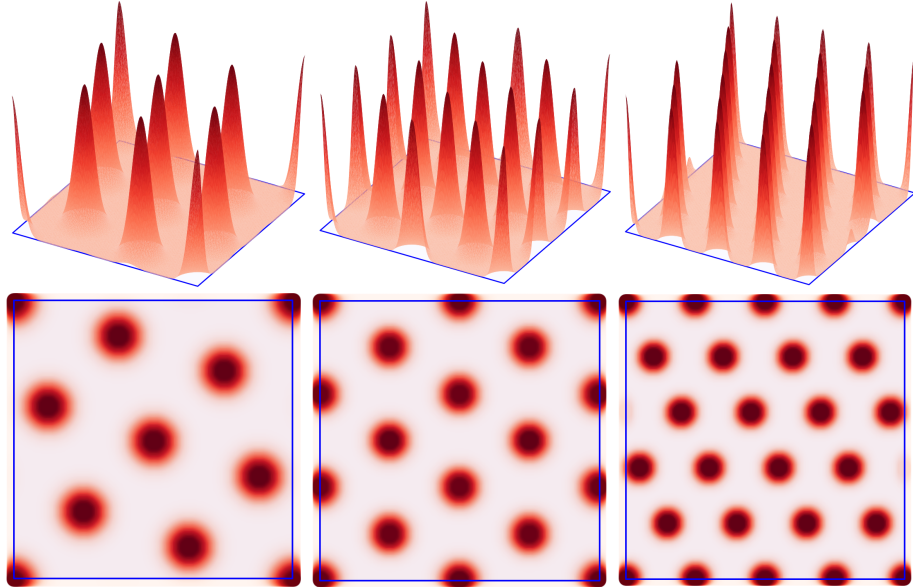


Fig. 3 The density profiles of 8 (left panel), 12 (middle panel) and 20 (right panel) electrons confined to a 2D square Clifford supercell at $r_s = 105$. The profiles on the top show a view from the front while the profiles at the bottom show a view from above.

In the middle panel of Fig. 2 we report the density for 5 electrons confined to a square Clifford supercell. We observe that the electrons localise on two parallel lines, with each line joining a vertex to the center of an edge of the Clifford supercell. For both 3 and 5 electrons all electrons are equivalent but this is not always the case. For example, for 7 electrons confined to a square Clifford supercell there are 4 inequivalent electrons. We report this result in the right panel of Fig. 2. There are 4 types of density distributions around the center of a localised electron that differ slightly in their amplitudes and widths. Moreover, some density distributions are anisotropic.

An interesting localisation pattern emerges in a Wigner fragment with 8 electrons confined to a square Clifford supercell reported in the left panel of Fig. 3. We see that the localised electrons form a distorted hexagonal lattice. Approximate hexagonal structures also emerge naturally in other square Clifford tori with more electrons such as $N = 12$ and $N = 20$. We report those density profiles in middle and right panels of Fig. 3.

In the above calculations the edges of the Clifford supercell were fixed to be equal, i.e., $L_x = L_y$. For such a Clifford supercell it is not possible to find a perfect hexagonal lattice because it is incommensurable with a square for any number of electrons. To verify if indeed a perfect hexagonal lattice will emerge, we now choose the ratio L_y/L_x and the number of electrons to be commensurable with the hexagonal lattice. To achieve this, we performed a calculation of 16 electrons confined to a rectangular Clifford supercell with $L_y/L_x = \sqrt{3}/2$. We used 418 gaussians on a 22×19 grid.

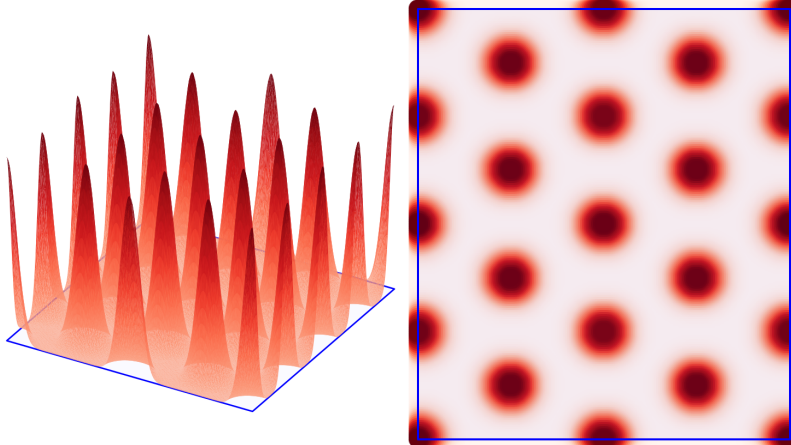


Fig. 4 The density profiles of 16 electrons confined to a 2D square Clifford supercell commensurable with the hexagonal lattice at $r_s = 105$. The profile on the left shows a view from the front while the profile on the right shows a view from above.

The corresponding density profile can be found in Fig. 4. We obtain a perfect hexagonal lattice that demonstrates the emergence of the hexagonal structure in a uniform electron gas at low density.

We have calculated the density profiles of Wigner fragments for N electrons in a square Clifford supercell for all values of N up to $N = 20$. All those results are reported in the appendix for completeness. Finally, at vanishing average density the kinetic energy contribution will become negligible with respect to the Coulomb repulsion. Therefore, we expect that in this limit the positions at which the electrons localise will be equivalent to the positions for which classical point charges obtain their minimal energy. We have numerically verified that this is indeed the case. This comparison between the quantum and classical results can also be found in the appendix.

Conclusions and outlook

We have proposed an accurate and efficient approach to study two-dimensional Wigner fragments from first principles. It is based on the creation of a supercell that has the topology of a Clifford torus together with introduction of a renormalized distance in the Coulomb potential. Our approach is fully quantum mechanical and makes no assumptions on the positions where the electrons will localise. The density profiles we obtain, emerge naturally by minimising the total energy of the electrons confined to the fragments at low average density. Our results indicate that, for large numbers of electrons, a hexagonal lattice structure will emerge. We also conclude that, in general, not all the localised electrons are equivalent, even at very low density. Finally, our work paves the way for studying other interesting properties of Wigner fragments, such as their magnetic properties, by including the spin degrees of freedom. It could also be interesting to study three-dimensional Wigner fragments using the tools presented in this work.

Acknowledgments. We thank the French “Agence Nationale de la Recherche (ANR)” for financial support (Grant Agreements No. ANR-19-CE30-0011 and ANR-22-CE29-0001). This work has been (partially) supported through the EUR grant NanoX n° ANR-17-EURE-0009 in the framework of the “Programme des Investissements d’Avenir”.

Appendix A

The purpose of this section is two-fold: 1) we report all the density profiles we obtained for square two-dimensional Clifford supercells containing $N = 2, \dots, 20$ electrons. For convenience we also include those already reported in the main text. 2) We compare the density profiles to the positions of electrons in classical Wigner fragments. Since, in the limit of a vanishing average density, the kinetic energy contribution will become negligible with respect to the Coulomb repulsion, we expect that in this limit the positions at which the electrons localize will be equivalent to the positions for which classical point charges obtain their minimal energy. Therefore, we compare our quantum results for the equilibrium positions of the electrons to those obtained for a Clifford supercell with classical point charges. To determine these positions we minimize the energy of these classical Wigner fragments which is given by

$$U = \frac{1}{2} \sum_{i=1}^N \sum_{\substack{j=1 \\ j \neq i}}^N r_{ij}^{-1} \quad (\text{A1})$$

where r_{ij} is given in (2). We achieve this using the the conjugate-gradient method. Further details of our approach can be found in Ref. [15]. To simplify the comparison, the classical results are shown together with the their quantum analogs in Figs. A1-A19.

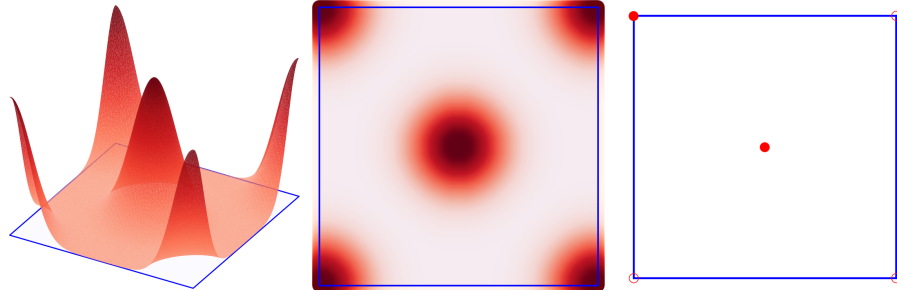


Fig. A1 The density for 2 electrons confined to a 2D square Clifford supercell at $r_s = 105$. Left panel: quantum results (front view); Middle panel: quantum result (top view); Right panel: classical result. Filled circles: the positions of the electrons; open circles: the equivalent positions of the electrons on the edge of the Clifford torus.

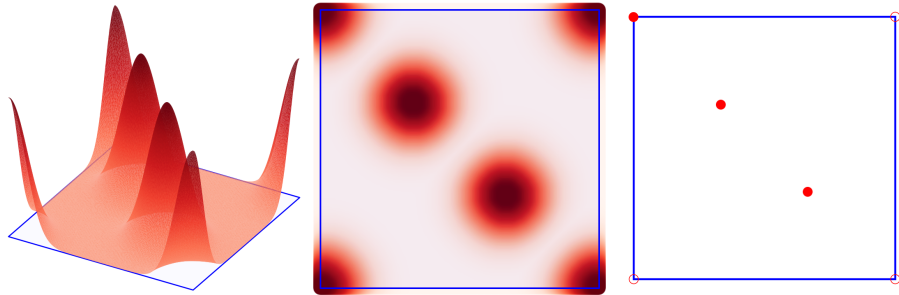


Fig. A2 The density for 3 electrons confined to a 2D square Clifford supercell at $r_s = 105$. Left panel: quantum results (front view); Middle panel: quantum result (top view); Right panel: classical result. Filled circles: the positions of the electrons; open circles: the equivalent positions of the electrons on the edge of the Clifford torus.

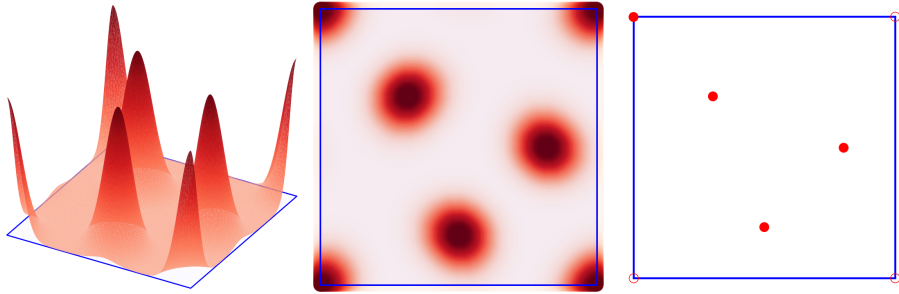


Fig. A3 The density for 4 electrons confined to a 2D square Clifford supercell at $r_s = 105$. Left panel: quantum results (front view); Middle panel: quantum result (top view); Right panel: classical result. Filled circles: the positions of the electrons; open circles: the equivalent positions of the electrons on the edge of the Clifford torus.

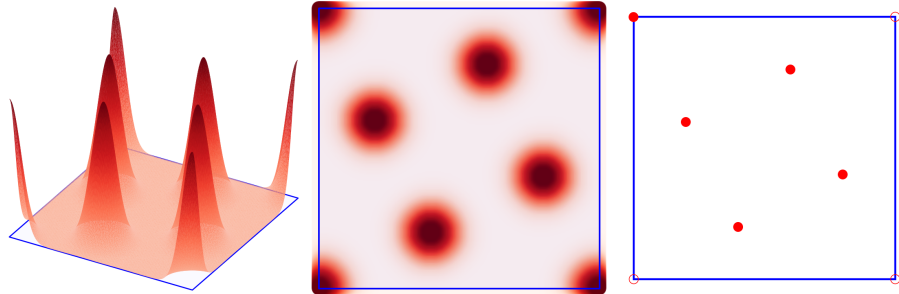


Fig. A4 The density for 5 electrons confined to a 2D square Clifford supercell at $r_s = 105$. Left panel: quantum results (front view); Middle panel: quantum result (top view); Right panel: classical result. Filled circles: the positions of the electrons; open circles: the equivalent positions of the electrons on the edge of the Clifford torus.

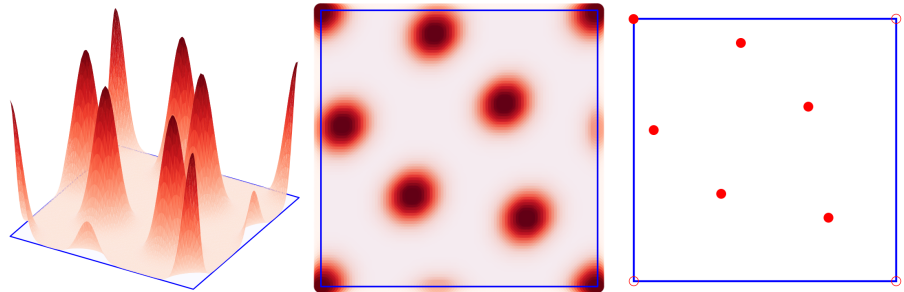


Fig. A5 The density for 6 electrons confined to a 2D square Clifford supercell at $r_s = 105$. Left panel: quantum results (front view); Middle panel: quantum result (top view); Right panel: classical result. Filled circles: the positions of the electrons; open circles: the equivalent positions of the electrons on the edge of the Clifford torus.

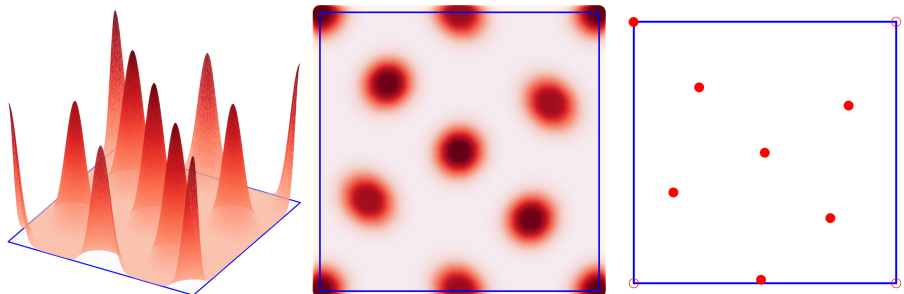


Fig. A6 The density for 7 electrons confined to a 2D square Clifford supercell at $r_s = 105$. Left panel: quantum results (front view); Middle panel: quantum result (top view); Right panel: classical result. Filled circles: the positions of the electrons; open circles: the equivalent positions of the electrons on the edge of the Clifford torus.

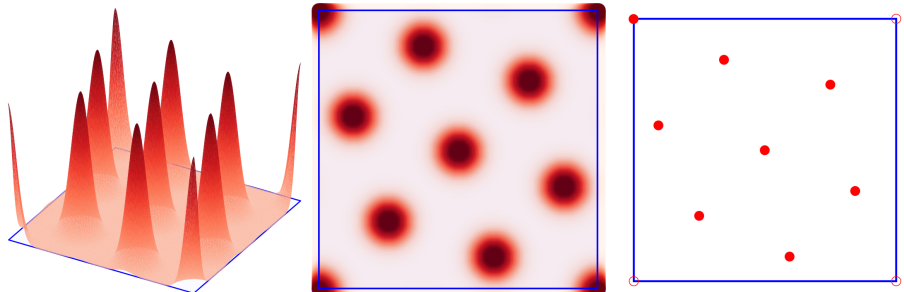


Fig. A7 The density for 8 electrons confined to a 2D square Clifford supercell at $r_s = 105$. Left panel: quantum results (front view); Middle panel: quantum result (top view); Right panel: classical result. Filled circles: the positions of the electrons; open circles: the equivalent positions of the electrons on the edge of the Clifford torus.

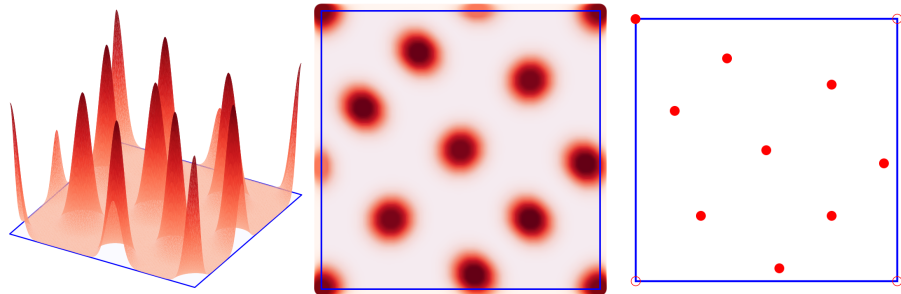


Fig. A8 The density for 9 electrons confined to a 2D square Clifford supercell at $r_s = 105$. Left panel: quantum results (front view); Middle panel: quantum result (top view); Right panel: classical result. Filled circles: the positions of the electrons; open circles: the equivalent positions of the electrons on the edge of the Clifford torus.

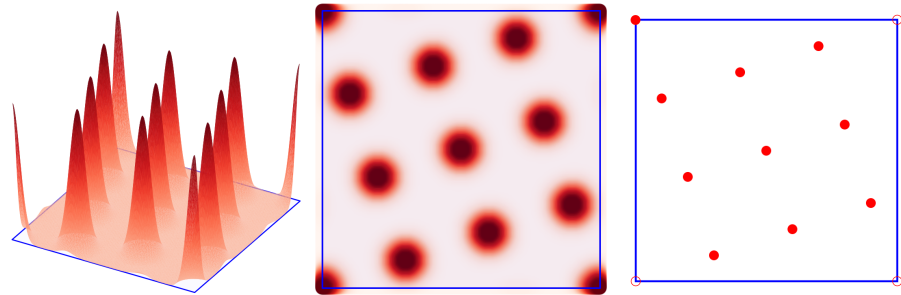


Fig. A9 The density for 10 electrons confined to a 2D square Clifford supercell at $r_s = 105$. Left panel: quantum results (front view); Middle panel: quantum result (top view); Right panel: classical result. Filled circles: the positions of the electrons; open circles: the equivalent positions of the electrons on the edge of the Clifford torus.

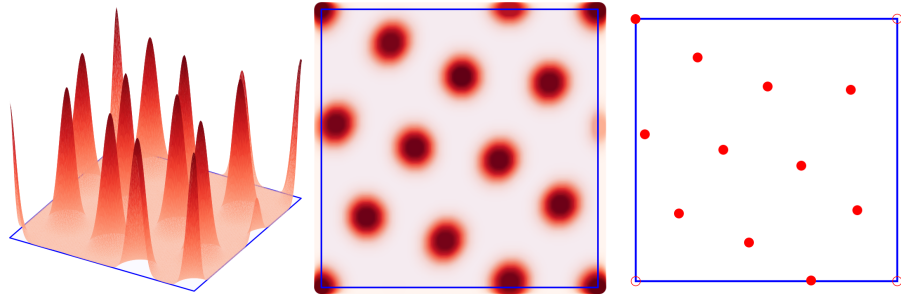


Fig. A10 The density for 11 electrons confined to a 2D square Clifford supercell at $r_s = 105$. Left panel: quantum results (front view); Middle panel: quantum result (top view); Right panel: classical result. Filled circles: the positions of the electrons; open circles: the equivalent positions of the electrons on the edge of the Clifford torus.

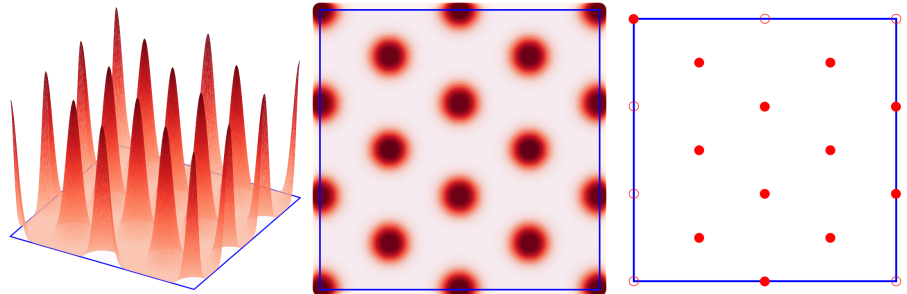


Fig. A11 The density for 12 electrons confined to a 2D square Clifford supercell at $r_s = 105$. Left panel: quantum results (front view); Middle panel: quantum result (top view); Right panel: classical result. Filled circles: the positions of the electrons; open circles: the equivalent positions of the electrons on the edge of the Clifford torus.

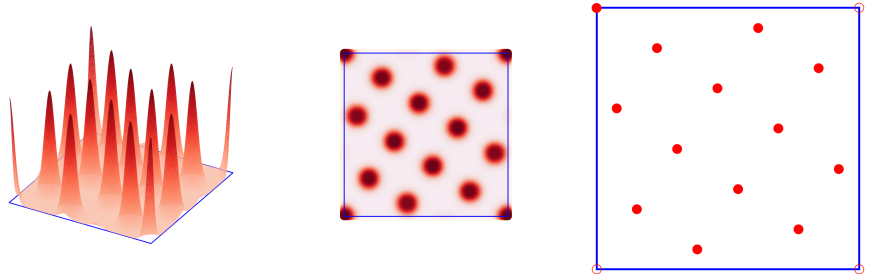


Fig. A12 The density for 13 electrons confined to a 2D square Clifford supercell at $r_s = 105$. Left panel: quantum results (front view); Middle panel: quantum result (top view); Right panel: classical result. Filled circles: the positions of the electrons; open circles: the equivalent positions of the electrons on the edge of the Clifford torus.

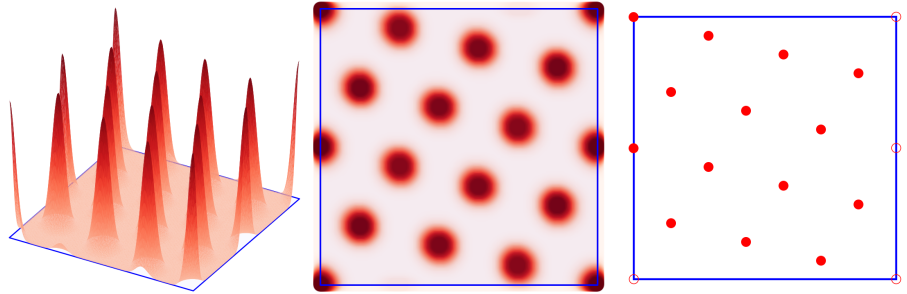


Fig. A13 The density for 14 electrons confined to a 2D square Clifford supercell at $r_s = 105$. Left panel: quantum results (front view); Middle panel: quantum result (top view); Right panel: classical result. Filled circles: the positions of the electrons; open circles: the equivalent positions of the electrons on the edge of the Clifford torus.

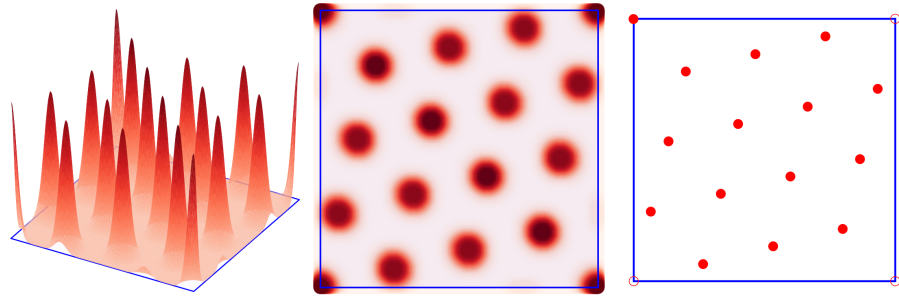


Fig. A14 The density for 15 electrons confined to a 2D square Clifford supercell at $r_s = 105$. Left panel: quantum results (front view); Middle panel: quantum result (top view); Right panel: classical result. Filled circles: the positions of the electrons; open circles: the equivalent positions of the electrons on the edge of the Clifford torus.

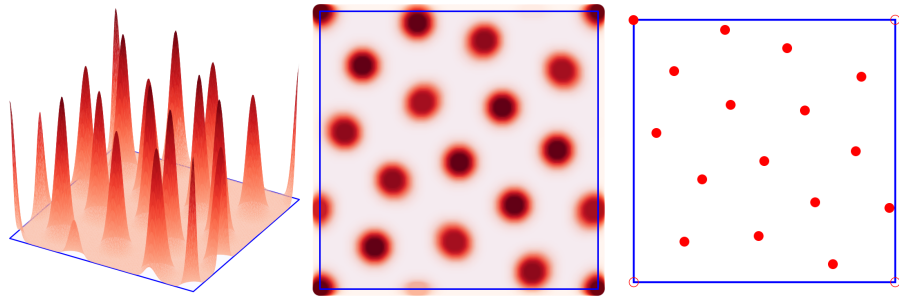


Fig. A15 The density for 16 electrons confined to a 2D square Clifford supercell at $r_s = 105$. Left panel: quantum results (front view); Middle panel: quantum result (top view); Right panel: classical result. Filled circles: the positions of the electrons; open circles: the equivalent positions of the electrons on the edge of the Clifford torus.

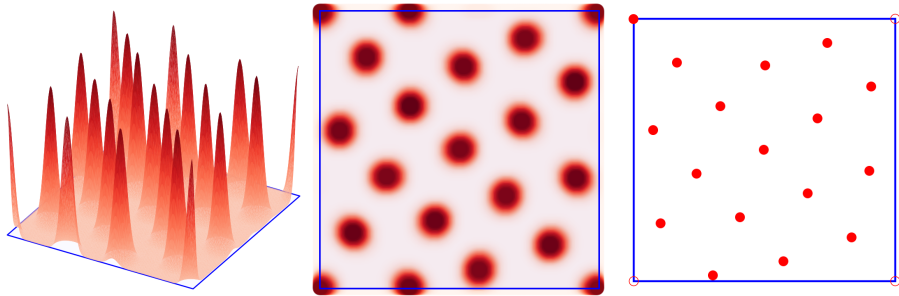


Fig. A16 The density for 17 electrons confined to a 2D square Clifford supercell at $r_s = 105$. Left panel: quantum results (front view); Middle panel: quantum result (top view); Right panel: classical result. Filled circles: the positions of the electrons; open circles: the equivalent positions of the electrons on the edge of the Clifford torus.

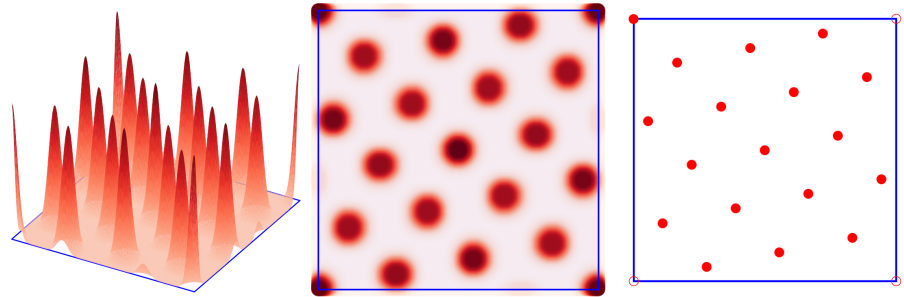


Fig. A17 The density for 18 electrons confined to a 2D square Clifford supercell at $r_s = 105$. Left panel: quantum results (front view); Middle panel: quantum result (top view); Right panel: classical result. Filled circles: the positions of the electrons; open circles: the equivalent positions of the electrons on the edge of the Clifford torus.

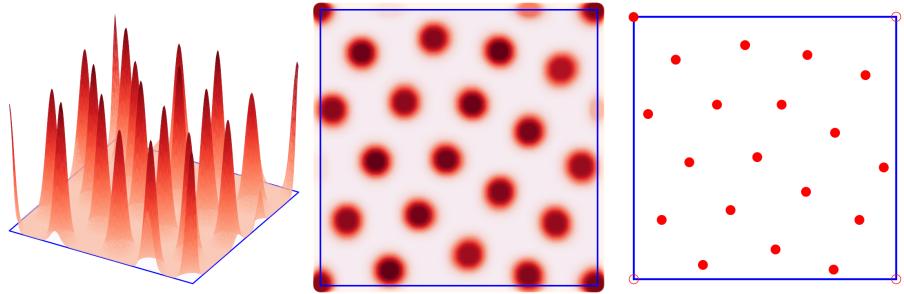


Fig. A18 The density for 19 electrons confined to a 2D square Clifford supercell at $r_s = 105$. Left panel: quantum results (front view); Middle panel: quantum result (top view); Right panel: classical result. Filled circles: the positions of the electrons; open circles: the equivalent positions of the electrons on the edge of the Clifford torus.

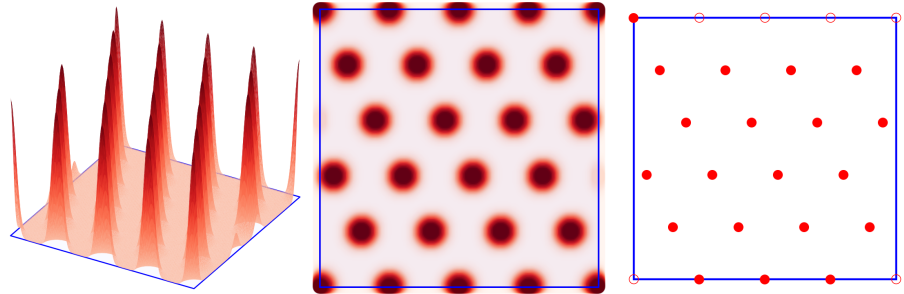


Fig. A19 The density for 20 electrons confined to a 2D square Clifford supercell at $r_s = 105$. Left panel: quantum results (front view); Middle panel: quantum result (top view); Right panel: classical result. Filled circles: the positions of the electrons; open circles: the equivalent positions of the electrons on the edge of the Clifford torus.

References

- [1] Smołeński, T. *et al.* Signatures of Wigner crystal of electrons in a monolayer semiconductor. *Nature* **595**, 53–57 (2021).
- [2] Wigner, E. On the interaction of electrons in metals. *Phys. Rev.* **46**, 1002–1011 (1934).
- [3] Tavernier, N., Bendazzoli, G. L., Brumas, V., Evangelisti, S. & Berger, J. A. Clifford boundary conditions: A simple direct-sum evaluation of Madelung constants. *J. Phys. Chem. Lett.* **11**, 7090–7095 (2020). URL <https://doi.org/10.1021/acs.jpclett.0c01684>.
- [4] Escobar Azor, M., Alves, E., Evangelisti, S. & Berger, J. A. Wigner localization in two and three dimensions: An ab initio approach. *J. Chem. Phys.* **155**, 124114 (2021). URL <https://doi.org/10.1063/5.0063100>.
- [5] Fuchs, K. & Fowler, R. H. A quantum mechanical investigation of the cohesive forces of metallic copper. *Proceedings of the Royal Society of London. Series A - Mathematical and Physical Sciences* **151**, 585–602 (1935).
- [6] Sholl, C. A. The calculation of electrostatic energies of metals by plane-wise summation. *Proceedings of the Physical Society* **92**, 434–445 (1967). URL <https://doi.org/10.1088/0370-1328/92/2/321>.
- [7] Bonsall, L. & Maradudin, A. A. Some static and dynamical properties of a two-dimensional Wigner crystal. *Phys. Rev. B* **15**, 1959–1973 (1977). URL <https://link.aps.org/doi/10.1103/PhysRevB.15.1959>.
- [8] Tanatar, B. & Ceperley, D. M. Ground state of the two-dimensional electron gas. *Phys. Rev. B* **39**, 5005–5016 (1989). URL <https://link.aps.org/doi/10.1103/PhysRevB.39.5005>.
- [9] Rapisarda, F. & Senatore, G. Diffusion Monte Carlo study of electrons in two-dimensional layers. *Aust. J. Phys.* **49**, 161–182 (1996).
- [10] Hasse, R. W. & Avilov, V. V. Structure and Madelung energy of spherical Coulomb crystals. *Phys. Rev. A* **44**, 4506–4515 (1991). URL <https://link.aps.org/doi/10.1103/PhysRevA.44.4506>.
- [11] Drummond, N. D., Radnai, Z., Trail, J. R., Towler, M. D. & Needs, R. J. Diffusion quantum Monte Carlo study of three-dimensional Wigner crystals. *Phys. Rev. B* **69**, 085116 (2004). URL <https://link.aps.org/doi/10.1103/PhysRevB.69.085116>.
- [12] Drummond, N. D. & Needs, R. J. Phase diagram of the low-density two-dimensional homogeneous electron gas. *Phys. Rev. Lett.* **102**, 126402 (2009). URL <https://link.aps.org/doi/10.1103/PhysRevLett.102.126402>.

- [13] Alves, E., Bendazzoli, G. L., Evangelisti, S. & Berger, J. A. Accurate ground-state energies of Wigner crystals from a simple real-space approach. *Phys. Rev. B* **103**, 245125 (2021). URL <https://link.aps.org/doi/10.1103/PhysRevB.103.245125>.
- [14] Giuliani, G. F. & Vignale, G. *Quantum theory of the electron liquid* (Cambridge University Press).
- [15] Alrakik, A. *et al.* Solution to the Thomson problem for Clifford tori with an application to Wigner crystals. *accepted in J. Chem. Theory Comput.*; *arXiv:2305.15604* (2023).
- [16] Lozovik, Y. & Yudson, V. Crystallization of a two-dimensional electron gas in a magnetic field. *J. Exp. Theor. Phys. Lett.* **22**, 11–12 (1975).
- [17] Grimes, C. C. & Adams, G. Evidence for a liquid-to-crystal phase transition in a classical, two-dimensional sheet of electrons. *Phys. Rev. Lett.* **42**, 795–798 (1979). URL <https://link.aps.org/doi/10.1103/PhysRevLett.42.795>.
- [18] Andrei, E. Y. *et al.* Observation of a magnetically induced wigner solid. *Phys. Rev. Lett.* **60**, 2765–2768 (1988). URL <https://link.aps.org/doi/10.1103/PhysRevLett.60.2765>.
- [19] Goldman, V. J., Santos, M., Shayegan, M. & Cunningham, J. E. Evidence for two-dimentional quantum Wigner crystal. *Phys. Rev. Lett.* **65**, 2189–2192 (1990). URL <https://link.aps.org/doi/10.1103/PhysRevLett.65.2189>.
- [20] Williams, F. I. B. *et al.* Conduction threshold and pinning frequency of magnetically induced Wigner solid. *Phys. Rev. Lett.* **66**, 3285–3288 (1991). URL <https://link.aps.org/doi/10.1103/PhysRevLett.66.3285>.
- [21] Ye, P. D. *et al.* Correlation lengths of the wigner-crystal order in a two-dimensional electron system at high magnetic fields. *Phys. Rev. Lett.* **89**, 176802 (2002). URL <https://link.aps.org/doi/10.1103/PhysRevLett.89.176802>.
- [22] Chen, Y. P. *et al.* Melting of a 2d quantum electron solid in high magnetic field. *Nat. Phys.* **2**, 452–455 (2006).
- [23] Jang, J., Hunt, B. M., Pfeiffer, L. N., West, K. W. & Ashoori, R. C. Sharp tunnelling resonance from the vibrations of an electronic Wigner crystal. *Nature Physics* **13**, 340–344 (2017). URL <https://doi.org/10.1038/nphys3979>.
- [24] Regan, E. C. *et al.* Mott and generalized Wigner crystal states in wse₂/ws₂ moiré superlattices. *Nature* **579**, 359–363 (2020). URL <https://doi.org/10.1038/s41586-020-2092-4>.
- [25] Tang, Y. *et al.* Simulation of hubbard model physics in wse₂/ws₂ moiré superlattices. *Nature* **579**, 353–358 (2020). URL <https://doi.org/10.1038/s41586-020-2092-4>.

s41586-020-2085-3.

- [26] Xu, Y. *et al.* Correlated insulating states at fractional fillings of moiré superlattices. *Nature* **587**, 214–218 (2020).
- [27] Li, H. *et al.* Imaging two-dimensional generalized Wigner crystals. *Nature* **597**, 650–654 (2021). URL <https://doi.org/10.1038/s41586-021-03874-9>.
- [28] Cioslowski, J. & Buchowiecki, M. Wigner molecules: Natural orbitals of strongly correlated two-electron harmonium. *J. Chem. Phys.* **125**, 064105 (2006).
- [29] Ellenberger, C. *et al.* Excitation spectrum of two correlated electrons in a lateral quantum dot with negligible zeeman splitting. *Phys. Rev. Lett.* **96**, 126806 (2006). URL <https://link.aps.org/doi/10.1103/PhysRevLett.96.126806>.
- [30] Yannouleas, C. & Landman, U. Symmetry breaking and quantum correlations in finite systems: studies of quantum dots and ultracold bose gases and related nuclear and chemical methods. *Rep. Prog. Phys.* **70**, 2067–2148 (2007). URL <https://doi.org/10.1088/0034-4885/70/12/r02>.
- [31] Mendl, C. B., Malet, F. & Gori-Giorgi, P. Wigner localization in quantum dots from Kohn-Sham density functional theory without symmetry breaking. *Phys. Rev. B* **89**, 125106 (2014). URL <https://link.aps.org/doi/10.1103/PhysRevB.89.125106>.
- [32] Cioslowski, J. One-electron densities of freely rotating Wigner molecules. *J. Phys. B: At. Mol. Opt. Phys.* **50**, 235102 (2017).
- [33] Cioslowski, J. & Strasburger, K. Harmonium atoms at weak confinements: The formation of the Wigner molecules. *J. Chem. Phys.* **146**, 044308 (2017).
- [34] Egger, R., Häusler, W., Mak, C. H. & Grabert, H. Crossover from fermi liquid to wigner molecule behavior in quantum dots. *Phys. Rev. Lett.* **82**, 3320–3323 (1999).
- [35] Diaz-Marquez, A. *et al.* Signatures of Wigner localization in one-dimensional systems. *J. Chem. Phys.* **148**, 124103 (2018).
- [36] Telleria-Allika, X. *et al.* The Wigner localization of interacting electrons in a one-dimensional harmonic potential. *J. Chem. Phys.* **157**, 174107 (2022).
- [37] Escobar Azor, M. *et al.* A Wigner molecule at extremely low densities: a numerically exact study. *SciPost Physics Core* **1**, 001 (2019).
- [38] Pecker, S. *et al.* Observation and spectroscopy of a two-electron Wigner molecule in an ultraclean carbon nanotube. *Nature Physics* **9**, 576–581 (2013). URL <https://doi.org/10.1038/nphys2692>.

- [39] Méndez-Camacho, R. & Cruz-Hernández, E. Asymmetric Wigner molecules in nanowire y-junctions. *Scientific Reports* **12**, 20183 (2022). URL <https://doi.org/10.1038/s41598-022-24583-x>.
- [40] Méndez-Camacho, R. & Cruz-Hernández, E. Tunneling between parallel one-dimensional Wigner crystals. *Scientific Reports* **12**, 4470 (2022). URL <https://doi.org/10.1038/s41598-022-08367-x>.
- [41] Thakur, T. & Szafran, B. Wigner molecules in phosphorene quantum dots. *Phys. Rev. B* **106**, 205304 (2022). URL <https://link.aps.org/doi/10.1103/PhysRevB.106.205304>.
- [42] Tavernier, N., Bendazzoli, G. L., Brumas, V., Evangelisti, S. & Berger, J. A. Clifford boundary conditions for periodic systems: the Madelung constant of cubic crystals in 1, 2 and 3 dimensions. *Theor. Chem. Acc.* **140**, 106 (2021).
- [43] Malet, F., Mirtschink, A., Cremon, J. C., Reimann, S. M. & Gori-Giorgi, P. Kohn-Sham density functional theory for quantum wires in arbitrary correlation regimes. *Phys. Rev. B* **87**, 115146 (2013).
- [44] Brooke, L. *et al.* Distributed gaussian orbitals for the description of electrons in an external potential. *J. Mol. Model.* **24**, 216 (2018).
- [45] Aidas, K. *et al.* The Dalton quantum chemistry program system. *WIREs Computational Molecular Science* **4**, 269–284 (2014). URL <https://wires.onlinelibrary.wiley.com/doi/abs/10.1002/wcms.1172>.
- [46] Hegarty, D. & Robb, M. A. Application of unitary group methods to configuration interaction calculations. *Mol. Phys.* **38**, 1795–1812 (1979).